Energy & Environmental Science

www.rsc.org/ees

Volume 6 | Number 3 | March 2013 | Pages 681–1048

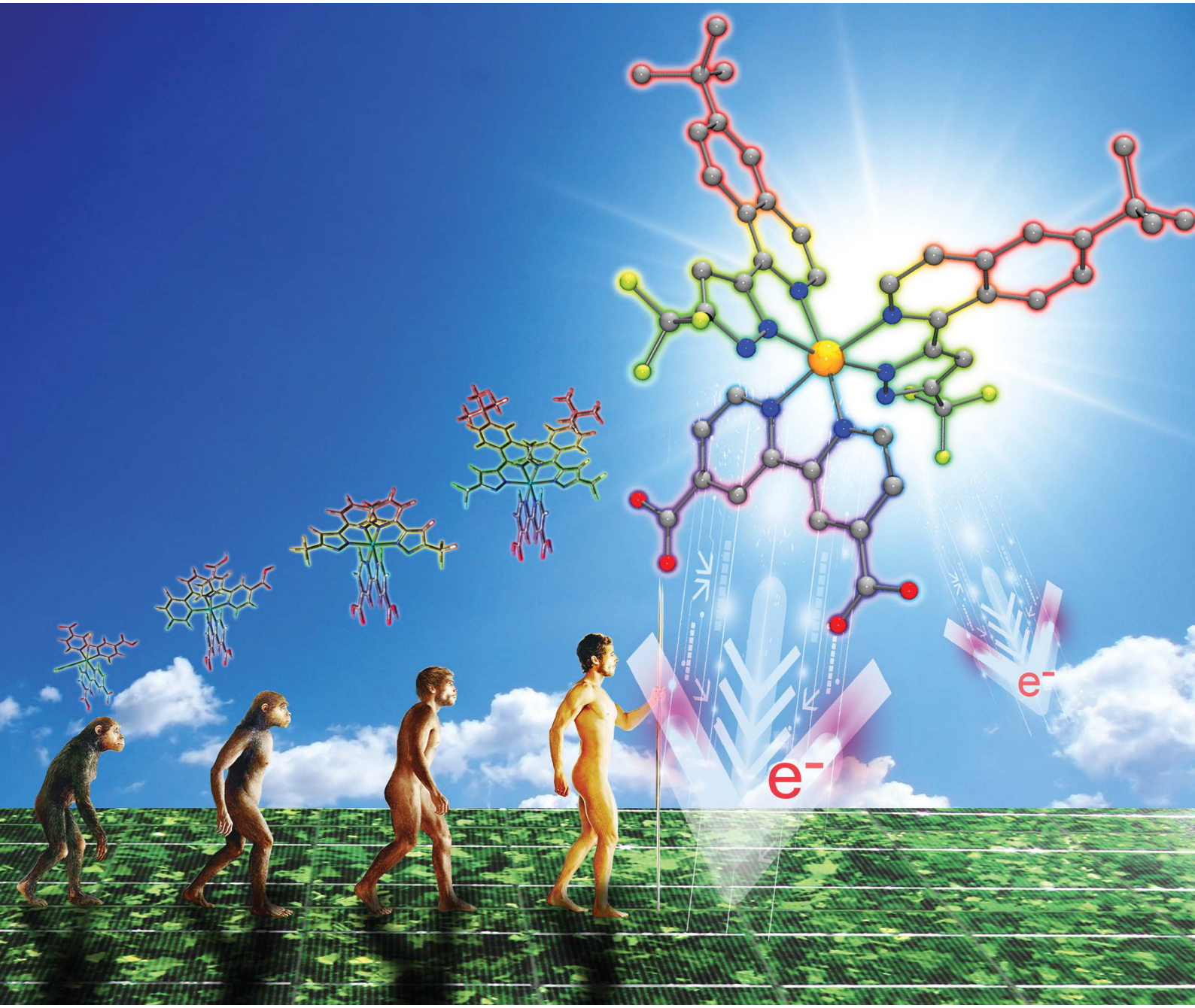

ISSN 1754-5692

RSC Publishing

PAPER

Yun Chi *et al.*

Harnessing the open-circuit voltage *via* a new series of Ru(II) sensitizers bearing (*iso*-)quinolinyl pyrazolate ancillaries

1754-5692(2013)6:3;1-1

Energy & Environmental Science

RSC Publishing

PAPER

Cite this: *Energy Environ. Sci.*, 2013, **6**, 859

Harnessing the open-circuit voltage *via* a new series of Ru(II) sensitizers bearing (*iso*-)quinolinyl pyrazolate ancillaries†

Kuan-Lin Wu,‡[ae] Wan-Ping Ku,‡[a] John N. Clifford,*[b] Emilio Palomares,[bc] Shu-Te Ho,[a] Yun Chi,*[a] Shih-Hung Liu,[d] Pi-Tai Chou,*[d] Mohammad K. Nazeeruddin*[e] and Michael Grätzel[e]

Received 6th November 2012
Accepted 7th January 2013

DOI: 10.1039/c2ee23988d

www.rsc.org/ees

A novel class of Ru(II) sensitizers (TFRS-51–TFRS-54) with a 4,4′-dicarboxy-2,2′-bipyridine anchoring ligand and two *trans*-oriented isoquinolinyl (or quinolinyl) pyrazolate ancillaries were designed, characterized and used to fabricate dye sensitized solar cell (DSC) devices. In sharp contrast to Ru(II) sensitizers that employ functionalized thiophene appendages in their ancillary bipyridal ligands, the extended π-conjugation introduced by the isoquinolinyl or quinolinyl groups improves the optical absorptivity, particularly for the absorption located at ~500 nm when compared with the parent sensitizer TFRS-1 possessing less conjugated 5-pyrid-2-yl pyrazolate ancillaries. As a result, DSCs incorporated with these dyes show much improved J_{SC} compared with the reference device. Moreover, the use of bulky *t*-butyl substituents on the ancillary ligands improves the cell performance with excellent V_{OC} of up to 830 mV recorded. Also, the addition of tetra-*n*-butyl ammonium deoxycholate [TBA][DOC] as co-adsorbent to the dye solution further improves the power conversion efficiency (η). The best solar cell parameters recorded were J_{SC} = 16.3 mA cm^{-2}, V_{OC} = 860 mV, FF = 0.72, and η = 10.1% for a device sensitized with TFRS-52. The markedly high open-circuit voltage is confirmed by the longer electron lifetime revealed in transient photovoltage (TPV) measurement *versus* the TFRS-1 sensitizer, and is probably derived from a combination of the higher conduction band edge of TiO_2 induced by the *in situ* metathesis of carboxylate anchors and the reduced recombination contributed by the bulky sensitizer.

Broader context

The dye-sensitized solar cell (DSC) has been considered to be one of the best photovoltaic technologies in virtue of the ecological motivations and cost related issues. In the present article, we declared that the short circuit current of DSC can be increased *via* addition of fused aromatic substituents (*i.e.* isoquinolinyl groups) on the polypyridyl Ru(II) sensitizers, which is complementary to the traditional method of incorporating thiophene pendant. Furthermore, the open circuit voltage of DSC was also boosted *via* simultaneous increase of the Fermi energy level of TiO_2 by employment of the carboxylate anchors, as well as by attachment of *t*-butyl group on the ancillary chelates; the latter is capable for suppressing electron recombination *via* steric effect. With a recorded efficiency of over double digits, this work illustrates a practical strategy to achieve highly efficient DSCs for future applications.

[a]*Department of Chemistry and Low Carbon Energy Research Center, National Tsing Hua University, Hsinchu 30013, Taiwan. E-mail: ychi@mx.nthu.edu.tw*

[b]*Institute of Chemical Research of Catalonia (ICIQ), Avda. Països Catalans 16, 43007 Tarragona, Spain. E-mail: jnclifford@iciq.es*

[c]*ICREA, Avda. Lluís Companys 28, Barcelona E-08030, Spain*

[d]*Department of Chemistry and Center for Emerging Material and Advanced Devices, National Taiwan University, Taipei 10617, Taiwan. E-mail: chop@ntu.edu.tw*

[e]*Ecole polytechnique fédérale de Lausanne, Institute of Chemical Sciences and Engineering, Laboratory of Photonics and Interfaces, 1015 Lausanne, Switzerland. E-mail: mdkhaja.nazeeruddin@epfl.ch*

† Electronic supplementary information (ESI) available: Figures and tables showing the absorption spectrum and selected electronic transitions obtained using the TD-DFT PCM calculations in DMF, figures containing transient absorption and transient photovoltage decays of TFRS-51–TFRS-54, and the cell performance of TFRS-52. See DOI: 10.1039/c2ee23988d

‡ K.L.W. and W.P.K. contributed equally to this work.

During the past two decades, Ru(II) based metal complexes, in particular those possessing di- or tri-carboxy substituted polypyridine chelates, have attracted much attention in the development of dye-sensitized solar cells (DSCs).[1] Their easily tunable redox and photophysical properties and proven stability triggered the synthesis of hundreds of novel Ru(II) derivatives.[2,3] Moreover, the absorption onset of Ru(II) sensitizers is notably red-shifted *versus* those of typical organic push–pull sensitizers,[3–5] which is attributed to the characteristic metal-to-ligand charge transfer (MLCT) transitions and allows for higher short circuit photocurrent (J_{SC}) due to the effective harvesting of solar irradiation down to the deep red region. The pioneering works of Grätzel and coworkers have established two paradigms for highly efficient Ru(II) sensitizers, namely **N719** and **N749**.[6–8] As

shown in Scheme 1, the red colored **N719** sensitizer is composed of two 4,4-dicarboxy-2,2′-bipyridine chelates together with two *cis*-substituted thiocyanates, while the dark-green colored N749 is assembled using a highly conjugated 4,4′,4″-tricarboxy-2,2′:6,2″-terpyridine plus three thiocyanate ancillaries, so that its absorption onset can be extended further into the near-infrared region.

Despite their excellent light-harvesting abilities, the low molar extinction coefficients of **N719** and **N749** (for example, in ethanol solvent ε for **N719** is 13 900 M^{-1} cm^{-1} at 541 nm)[9] demand the use of thicker TiO_2 photoanodes in DSC devices to harvest all of the incident photons. Such a strategy results in increased recombination losses and unsatisfactory open-circuit voltages (V_{OC}) and, in turn, limits the overall conversion efficiency. This has encouraged synthetic chemists to work on the molecular engineering of the relevant sensitizers with the aim of increasing their absorptivity.[2,10–13] Typical strategies have involved the elongation of the conjugation length of either the anchoring carboxy chelate or the bipyridine ancillary. Among numerous examples in the literature, Cao *et al.*[14] and Chen *et al.*[15] reported the synthesis and performance of two new classes of functionalized Ru(II) complexes, for which the representative examples are **C101** and **CYC-B11**. The structures of **C101** and **CYC-B11** incorporate thiophene and hexylthiobithiophene substituted bipyridine, respectively, as the ancillary ligands. The respective DSCs showed J_{SC} of 17.75 and 20.05 mA cm^{-2}, V_{OC} of 749 and 743 mV, and fill factor (FF) of 0.78 and 0.77, yielding power conversion efficiencies (η) of 10.3 and 11.5%, respectively. Despite their excellent efficiencies, the notable decrease in V_{OC} compared to the parent **N719**-sensitized solar cells (830 mV)[16,17] indicated a certain deteriorating effect of the sulfur-containing appendages. In good agreement with this result, O'Regan *et al.*[18] suggested that the change in V_{OC} was likely correlated with the formation of non-negligible sulfur–iodine (or tri-iodide) interaction between the dye and electrolyte, the result of which then leads to accelerated electron recombination.[19] Bearing this in mind, we have designed a series of new Ru(II) complexes, in which the absorptivity is enhanced solely by fused chromophores without any sulfur atom. This strategy, in principle, may result in less significant interaction with either iodine or tri-iodide in the electrolyte.[20–23] As elaborated below, these new Ru(II) sensitizers bearing *trans*-oriented isoquinolinyl (or quinolinyl) pyrazolate ancillaries show superior performance, particularly with regard to their high open-circuit voltage.

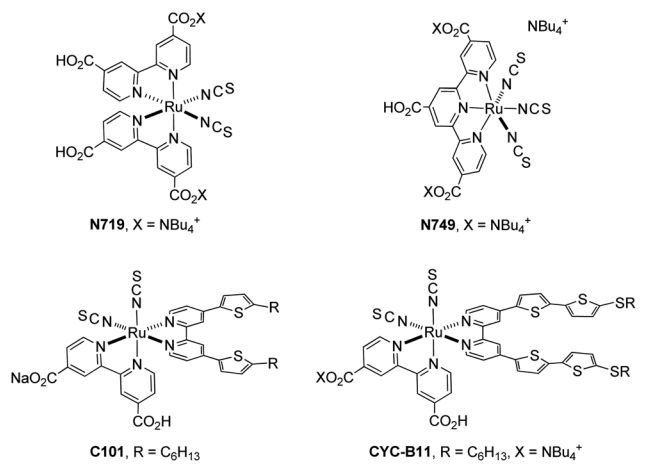

Scheme 1 Structural drawing of the Ru(II) sensitizers: **N719**, **N749**, **C101** and **CYC-B11**.

Results and discussion

Synthesis and structural characterization

For the synthesis of the ancillary ligands, acetylation of isoquinoline and quinoline was conducted using paraacetaldehyde in the presence of $FeSO_4 \cdot 7H_2O$, *t*-BuO_2H and trifluoroacetic acid.[24] Subsequent conversion to pyrazole was achieved employing Claisen condensation with ethyl trifluoroacetate, followed by treatment with hydrazine hydrate in ethanol.[25] The respective synthetic protocols are depicted in Scheme 2. In addition, it is well understood that the planar geometry of fused aromatics has a strong tendency to engage and afford inter- or intra-molecular π–π stacking interaction in the condensed phases. Using the Pt(II) and Ru(II) complexes as examples, Kato *et al.*[26] and Johansson *et al.*[27] reported the favorable formation of close contact for either isoquinolinyl or quinolinyl fragments *via* spectroscopy as well as X-ray diffraction studies. Further statistical analysis on quinoline based ligands using Cambridge Structural Database also confirmed their common occurrence.[28] As such, the heteroaromatics with bulky substituents, namely 6-*t*-butyl isoquinoline and quinoline, were next synthesized according to the literature procedures.[29,30] The respective chelating pyrazoles show much reduced propensity to aggregate.

The ancillary ligands were then treated with Ru(diethyl 2,2′-bipyridine-4,4′-dicarboxylate)(*p*-cymene)Cl in refluxing xylenes, followed by flash column chromatography and hydrolysis, yielding complexes TFRS-51–TFRS-54 in moderate yields, together with the isolation of one undesired (*i.e.* less efficient) stereoisomer. Their structural drawings are depicted in Scheme 3, together with that of the parent sensitizer TFRS-1.[31] It is notable that the pyrazolate fragments are all located at the mutual *trans*-disposition; this result is reminiscent of the bis-pyrazolate Ru(II) complexes that carry two *cis*-carbonyl ligands rather than the bipyridine.[32] Syntheses of these TFRS Ru(II)

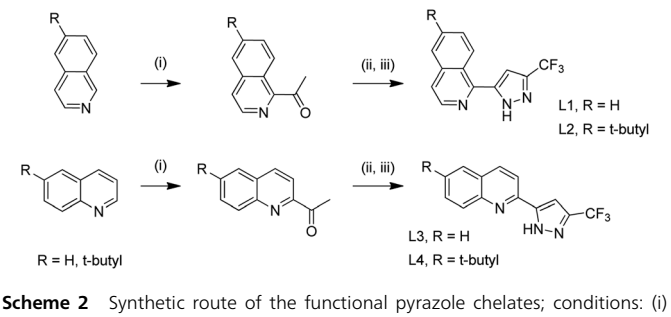

Scheme 2 Synthetic route of the functional pyrazole chelates; conditions: (i) $FeSO_4 \cdot 7H_2O$, paraacetaldehyde, *t*-BuO_2H, CF_3CO_2H, reflux; (ii) NaH, CF_3CO_2Et, THF; (iii) N_2H_4, reflux.

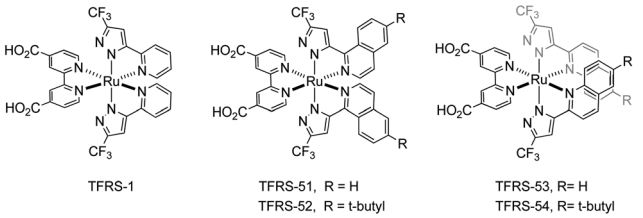

Scheme 3 Structural drawing of Ru(II) sensitizers TFRS-1 and TFRS-51–TFRS-54.

complexes also represent a fraction of our current endeavors aimed at designing more efficient and robust thiocyanate-free metal based DSC sensitizers.[33–35]

Photophysical and electrochemical behaviors

The absorption spectra of TFRS-51–TFRS-54 dyes are depicted in Fig. 1 together with that of TFRS-1. Pertinent photophysical and electrochemical properties are summarized in Table 1. In contrast to TFRS-1, which exhibits two absorption peaks at 405 and 515 nm, TFRS-51–TFRS-54 show a weak peak at near 430 nm, followed by another much intense and broadened absorption near 500 nm. Both bathochromic and hyperchromic effects displayed by these TFRS sensitizers are somewhat equivalent to the traditional method that employed functionalized thiophene appendage.[36] As supported by DFT calculations (see ESI†), the 500 nm band originates from the transition from Ru(II) core or the chelating pyrazolate to dicarboxy bipyridine, *i.e.* a mixing of MLCT and LLCT transitions, in a way analogous to the spectral assignment made for similar sensitizers in a previous study.[31]

It is also intriguing to note that the intensity of this band for the isoquinolinyl analogues TFRS-51 and TFRS-52 is notably greater than that of the quinolinyl counterparts TFRS-53 and TFRS-54, a result that is attributed to the difference in molecular architecture.[37] This salient change in absorptivity can be examined *via* the variation of lower lying transition dipole obtained from the DFT calculation (see ESI†). The calculated results reveal that TFRS-51–TFRS-54 dyes all possess two major

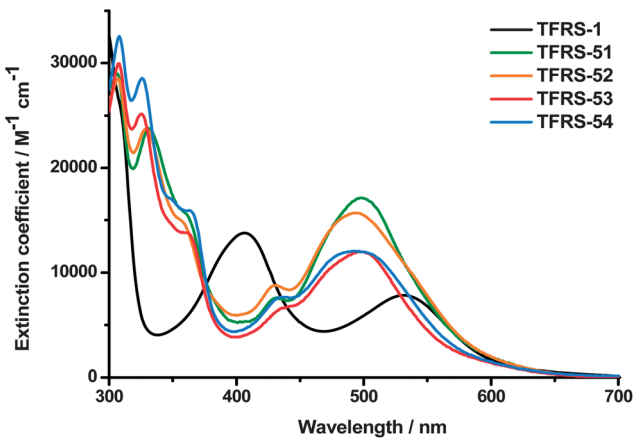

Fig. 1 UV/Vis spectra of TFRS sensitizers (1×10^{-5} M) in DMF.

Table 1 Photophysical and electrochemical data of the studied TFRS sensitizers in DMF

Dye	λ_{abs} [a] [nm] ($\varepsilon \times 10^{-3}$ [L mol^{-1} cm^{-1}])	$E_{ox}^{o'}$ [b]	E_{0-0} [c]	$E^{o'}$* [d]
TFRS-1	405 (15), 515 (9.1)	0.91	1.93	−1.02
TFRS-51	331 (24), 432 (7.6), 499 (17)	0.89	1.95	−1.06
TFRS-52	329 (24), 431 (8.8), 495 (16)	0.88	1.95	−1.07
TFRS-53	326 (25), 358 (14), 441 (6.7), 500 (12)	0.89	1.91	−1.02
TFRS-54	326 (29), 363 (16), 440 (7.7), 496 (12)	0.90	1.91	−1.01

[a] Molar extinction coefficients were measured in DMF solution. [b] Oxidation potential of dye was measured in DMF with 0.1 M [TBA][PF_6] and with a scan rate of 50 mV s^{-1}. It was calibrated with Fc/Fc^+ as internal reference and converted to NHE by addition of 0.63 V. [c] E_{0-0} was determined from the intersection of the absorption and the tangent of emission peak in DMF. [d] $E^{o'}$* was calculated as $E_{ox}^{o'} - E_{0-0}$.

transition peaks at ~460 and 540 nm, having significant oscillator strength of $f > 0.05$. Careful analyses of the corresponding frontier orbitals indicate that the ~540 and 460 nm peaks of all TFRS-51–TFRS-54 are mainly attributed to HOMO − 1 → LUMO and HOMO → LUMO + 1 transitions, respectively, in which the electron densities for both HOMO−1 and HOMO are distributed on Ru(II) d-orbitals and pyrazolate ligand, while that of LUMO and LUMO + 1 are mainly located at dicarboxy bipyridine, together with trace contributions from the Ru(II) metal core. While all TFRS-51–TFRS-54 sensitizers exhibit high oscillator strengths of $f = 0.12$–0.14 for the ~460 nm peak, the main difference between isoquinolinyl (TFRS-51 and -52) and quinolinyl (TFRS-53 and -54) analogues lies in the variation of MLCT percentage for the 540 nm band, in which MLCT percentage for TFRS-53 and TFRS-54 (>6%) are substantially larger than that of TFRS-51 and TFRS-52 (<2%). Accordingly, the more allowed ππ* transition percentage for isoquinolinyl analogues rationalizes the larger oscillator strength for TFRS-51 ($f = 0.122$ at 542.8 nm) and TFRS-52 ($f = 0.123$ at 546.3 nm) than that for TFRS-53 ($f = 0.068$ at 535.9 nm) and TFRS-54 ($f = 0.073$ at 539.1 nm). Since the experimentally resolved absorption band, in theory, can be simulated by the combination of the calculated 540–460 nm peaks, together with the consideration of vibronic transitions and inhomogeneous broadening in condensed phase, the larger absorptivity in TFRS-51 and TFRS-52 than that of TFRS-53 and TFRS-54 is thus supported. The calculation also indicates that the control TFRS-1 sensitizer possesses two lower lying major peaks at 567 and 468 nm with smaller oscillator strengths, being 0.06 and 0.10, respectively, due to less ππ* contribution,[24] which is consistent with the experimental results that its absorptivity is lower than that of TFR-51–TFRS-54 ($f > 0.06$ and 0.12 for ~540 and 460 nm bands, see Fig. 1 and ESI†). Finally, these UV/Vis spectra also indicate that the addition of *t*-butyl substituents to the isoquinolinyl and quinolinyl groups does not induce any significant change in the absorption profiles, which are evidenced by the resemblance of the UV/Vis spectra between TFRS-51/52 pair and TFRS-53/54 pair.

Cyclic voltammetry was conducted in DMF solution to verify whether the ground and excited oxidation potentials of the novel TFRS complexes are suitable for fabrication of TiO_2 based DSCs with iodide-containing redox electrolytes. As shown in

Table 1, all their oxidation potentials appeared at ~0.90 V (*vs.* NHE), which are comparable to that of the I_2^{-}/I^{-} redox potential (<0.79–0.93 V), but are more positive than that of the I^{-}/I_3^{-} redox couple (*ca.* 0.4 V *vs.* NHE).[38] The small variation of $E^{\circ'}_{ox}$ potentials among all complexes could be attributed to the identical inner environment for the Ru(II) metal complexes. Moreover, the oxidation potentials at the excited state ($E^{\circ'}$* = −1.01 to −1.07 V; see Table 1), estimated from the difference of $E^{\circ'}_{ox}$ and onset of the optical energy gap E_{0-0}, are also considered to be sufficiently more negative than that of the conduction band edge of the TiO_2 electrode (*ca.* −0.5 V *vs.* NHE).

Device performance characteristics

Devices were first fabricated using the as-prepared TFRS sensitizers, for which the device parameters measured under full sunlight irradiation (AM 1.5G, 100 mW cm^{-2}) are summarized in Table 2. The corresponding cells were prepared using a 0.4 × 0.4 cm^2 double layered TiO_2 film, which consisted of a transparent 12 μm absorption layer (20 nm) and a 6 μm scattering layer (400 nm), stained with a 0.3 mM dye solution in absolute ethanol and 20% (v/v) of DMSO for 16 h. The electrolyte solution consisted of 0.6 M DMPII, 0.05 M I_2, 0.5 M *t*-butylpyridine (TBP) in a 15 : 85 (v/v) mixture of valeronitrile and acetonitrile. The TFRS-1 device exhibited a J_{SC} of 12.6 mA cm^{-2}, V_{OC} of 780 mV, and FF of 0.76, corresponding to a η of 7.47%. We note that the efficiency is slightly lower than that reported for this dye in a previous study,[31] for which the previous cell performance data was recorded using different electrolytes and without a shading mask. For further confirmation of the performance data of TFRS-1, an independent study at EPFL gave J_{SC} of 14.21 mA cm^{-2}, V_{OC} of 830 mV, and FF of 0.75, corresponding to a η of 8.85%. Also, under identical conditions, the N719 sensitizer gave cell efficiencies of J_{SC} of 14.39 mA cm^{-2}, V_{OC} of 789 mV, and FF of 0.756, corresponding to a η of 8.58%. The performance data of these comparative experiments are summarized in the ESI.†

Cells fabricated using sensitizers TFRS-51 and TFRS-53 provide similar device efficiencies, except that TFRS-51 shows a notably higher J_{SC} that could be attributed to the higher molar extinction coefficient. The analogues of TFRS-51 and TFRS-53 that possess additional *t*-butyl substituents (*i.e.* TFRS-52 and TFRS-54) also show improved J_{SC} values and an enhancement in device performance, in particular the TFRS-52 that shows an overall efficiency of 9.05%. Especially notable are the high V_{OC} values recorded for the TFRS-52 and TFRS-54 devices, which are 40–50 mV higher than that reported for champion cells for **C101** by Cao *et al.*[14] and 80–90 mV higher than that reported for **CYC-B11** by Chen *et al.*,[15] though it should be pointed out that in these studies the electrolyte was not the same as the one used in our current work.

The above performance data indicate that the increase in π-conjugation without use of heteroatom appendages having a high propensity to bind iodide–tri-iodide redox couple, together with the bulky substituent such as the *t*-butyl group, provides an effective strategy to increase light absorption and J_{SC} whilst avoiding any trade-off by lowering V_{OC} due to increased recombination (*vide infra*). A similar concept of incorporating the nitrogen-containing heterocycles has been demonstrated in pure organic D–A–π–A sensitizers, in which linkers such as benzotriazole and quioxaline are known to induce a notable increase of open-circuit photovoltage *versus* other fragments.[39,40] Moreover, bulky and/or long alkyl chains employed in the metal-free organic sensitizers were also known to improve the DSC performances by reducing dye aggregation and effective blockage of charge recombination.[41–44]

In order to further optimize the devices, 2 eq. of tetra-*n*-butyl ammonium deoxycholate [TBA][DOC] co-adsorbent was added to the dye sensitizing solutions. It is believed that the metathesis of carboxylic acid/carboxylate anion of dyes can take place rapidly in dye solution.[45] This hypothesis is also confirmed by the examination of UV/Vis spectra of TFRS-52, both before and after the addition of [TBA][DOC]. As shown in Fig. 2, the absorption maximum at ~500 nm is slightly red-shifted upon addition of [TBA][DOC], and the lower energy shoulder experiences an opposite blue-shift. The latter can be explained by the fast deprotonation of 4,4′-dicarboxy-2,2′-bipyridine anchor, which is expected to enlarge the lower lying transition energy gap and to raise the oxidation potential of the excited sensitizer.

Moreover, for dyeing the TiO_2 with this modified dye solution, it is expected that both the absorbed sensitizer and deoxycholate can effectively transfer their excessive negative charge to the TiO_2 surface and consequently raise the respective

Table 2 DSC performances for cells fabricated using the TFRS sensitizers[a]

Dye	J_{SC} [mA cm^{-2}]	V_{OC} [mV]	FF	η [%]
TFRS-1	12.6	780	0.76	7.47
TFRS-51	13.5	750	0.76	7.71
TFRS-52	14.7	830	0.74	9.05
TFRS-53	12.4	750	0.77	7.12
TFRS-54	13.2	820	0.73	7.93

[a] The dye solution (0.3 mM) was prepared in absolute ethanol with 20% (v/v) of DMSO.

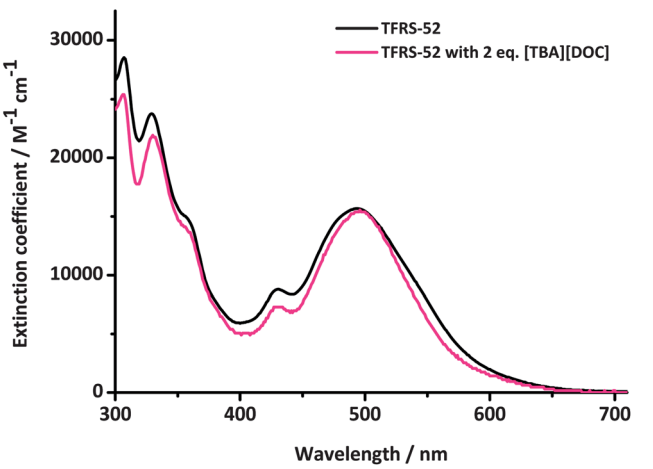

Fig. 2 UV/Vis spectra of TFRS-52 recorded before and after addition of 2 eq. [TBA][DOC] in DMF.

conducting band edge. In agreement with this hypothesis, DSCs fabricated using dye solutions containing [TBA][DOC] showed a significant increase in V_{OC} compared to DSC devices prepared without [TBA][DOC] (*c.f.* Tables 1 and 2). The highest efficiency was recorded with the TFRS-52 device of $J_{SC} = 16.3$ mAcm^{-2}, $V_{OC} = 860$ mV, FF = 0.72, and $\eta = 10.1\%$. For both TFRS-52 and TFRS-54, the V_{OC} reaches 860 mV, showing one of the highest values recorded for DSCs incorporating Ru(II) sensitizers. An independent study conducted in Grätzel's laboratory at EPFL also confirmed our result for TFRS-52 by giving a V_{OC} of 832 ± 2.8 mV and $\eta = 10.88 \pm 0.15\%$, for which the original data are compiled in the ESI.† Indeed, among the Ru(II) sensitizers for DSCs, the V_{OC} data of TFRS sensitizers were only exceeded by the fully deprotonated analogue of N719, $[Ru(dcbpy)_2(NCS)_2]$-$(Bu_4N)_4$ (N712), for which the V_{OC} has reached the limiting value of 900 mV, but with unavoidable suppression of J_{SC}.[46]

The incident photon-to-current conversion efficiencies (IPCEs) and the photocurrent density *vs.* voltage (*J*–*V*) curves of DSCs fabricated with the addition of [TBA][DOC] co-adsorbent are shown in Fig. 3a and b, respectively. The onsets of the IPCE spectra are all close to ~810 nm, and excellent IPCE performance was observed from 420 to 660 nm, among which the TFRS-51 and TFRS-53 show the maximum of 75.6% at 510 nm and 72.6% at 509 nm, while it increases to 75.4% at 517 nm and to 74.4% at 514 nm for TFRS-52 and TFRS-54, respectively. For a fair comparison, DSC fabricated using TFRS-1 showed slightly lower IPCE performance (*i.e.* light harvest efficiency) across the same range, revealing the superiority of the current sensitizers *versus* the parent sensitizer TFRS-1. The integration of IPCE spectral data from the region between 340 and 810 nm shows a deviation of ≤12% between the measured and calculated J_{SC}, which are within the expected range of errors (Table 3).

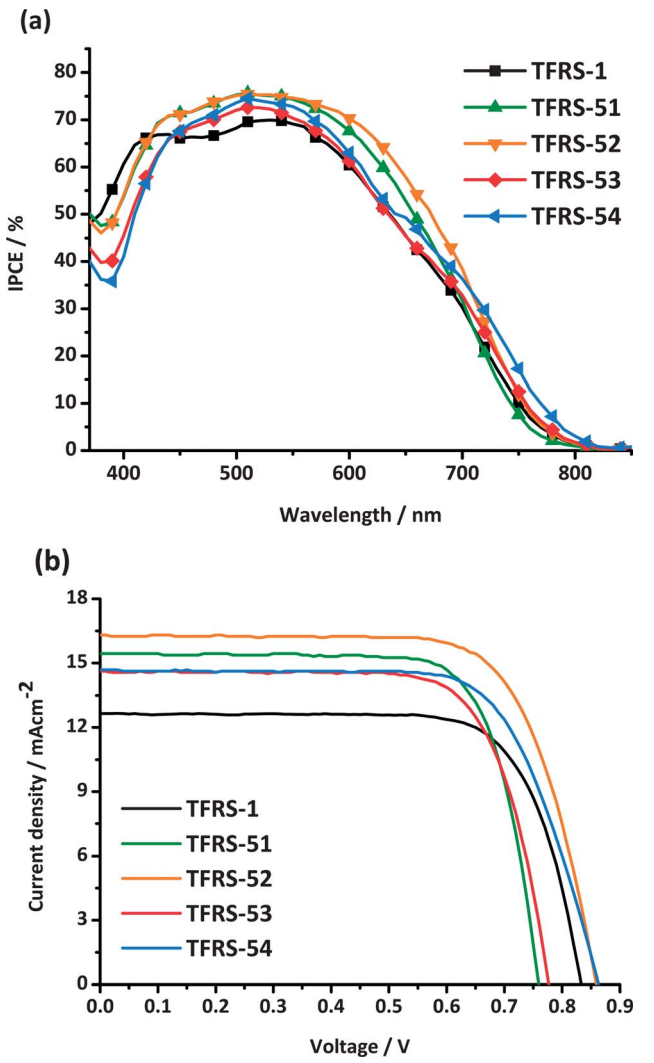

Fig. 3 (a) IPCE action spectra and (b) photocurrent density *vs.* voltage curves of studied DSC devices.

Photophysical measurements of DSC devices

To understand the different V_{OC} values for the DSCs prepared using [TBA][DOC] as co-adsorbent, electrochemical impedance spectroscopy (EIS), charge extraction (CE) and transient photovoltage (TPV) measurements were conducted. EIS is a powerful tool for investigating electronic and ionic transport processes in DSCs, which provides valuable information for the understanding of photovoltaic parameters. CE is used to study the amount of charge in a device under illumination. TPV measures the lifetime of electrons in devices under operational conditions and therefore the recombination lifetime. Fig. 4 shows the Nyquist plots measured under dark conditions at a forward bias of 850 mV. The high frequency arc is due to the resistance and capacitance at the platinum counter electrode, the intermediate frequency arc is the recombination resistance (R_{rec}) associated with electron recombination at the interface, combined with the chemical capacitance (C_{μ}) of electrons in TiO_2, and the low frequency arc is attributed to the impedance of diffusion of redox species in the electrolyte. The radii of the second series of semicircles indicates R_{rec} to be in the order of TFRS-52 > TFRS-1 > TFRS-51. A smaller R_{rec} value in theory means faster charge recombination between electrons in TiO_2 and electron acceptors in the electrolyte and thus shorter TiO_2 electron lifetimes.[47,48]

CE and TPV data indicate that voltage differences between these devices are due to both shifts in the TiO_2 conduction band edge and differences in TiO_2 electron lifetimes. The charge extraction and transient photovoltage data for devices composed of the TFRS sensitizers are shown in Fig. 5. TFRS-51–TFRS-54 devices all show higher electron densities than the TFRS-1 reference device, indicating a higher density of acceptor states due to a positive shift in the TiO_2 conduction band for these devices. TFRS-53 shows the largest shift whereas the others have intermediate shifts. This might imply lower voltages for TFRS-51–TFRS-54 devices but TiO_2 electron lifetimes (as determined by TPV) also influence V_{OC}. For these, TFRS-51 lifetimes are shorter than the reference TFRS-1 device explaining its lower V_{OC}. And though electron lifetimes for the TFRS-53 device are longer than for the TFRS-1 device, the shift in the conduction band is such that the V_{OC} of this device is still lower than TFRS-1. In sharp contrast, both TFRS-52 and TFRS-54 devices show much longer-lived electron lifetimes which must

Table 3 DSC performances for cells fabricated using dye solution with 2 eq. of [TBA][DOC] co-adsorbent

Dye	J_{SC} [mA cm^{-2}]	V_{OC} [mV]	FF	η [%]	Dye loading [mol cm^{-2}][a]
TFRS-1	12.7	830	0.74	7.84	5.28×10^{-7}
TFRS-51	15.4	760	0.75	8.80	3.31×10^{-7}
TFRS-52	16.3	860	0.72	10.1	3.22×10^{-7}
	16.8 ± 0.3	832 ± 2.8	0.78 ± 0.01	10.88 ± 0.15[b]	
TFRS-53	14.6	780	0.73	8.36	2.91×10^{-7}
TFRS-54	14.7	860	0.71	8.94	2.63×10^{-7}

[a] The dye loading on 12 + 6 μm TiO_2 films was desorbed in 0.1 M of TBAOH in 1 : 1 (v/v) mixture of MeOH and H_2O and then estimated using the UV/Vis spectral analysis. [b] These *J–V* characteristics were measured at the Laboratory of Photonics and Interfaces, Ecole Polytechnique Federale de Lausanne (EPFL) in Switzerland.

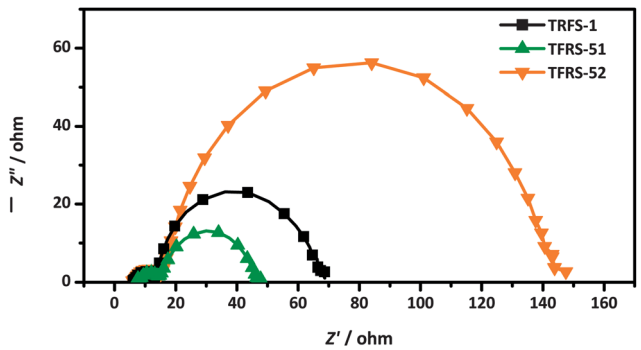

Fig. 4 Nyquist plots measured in the dark at a forward bias of 850 mV for the DSCs employing different TFRS dyes.

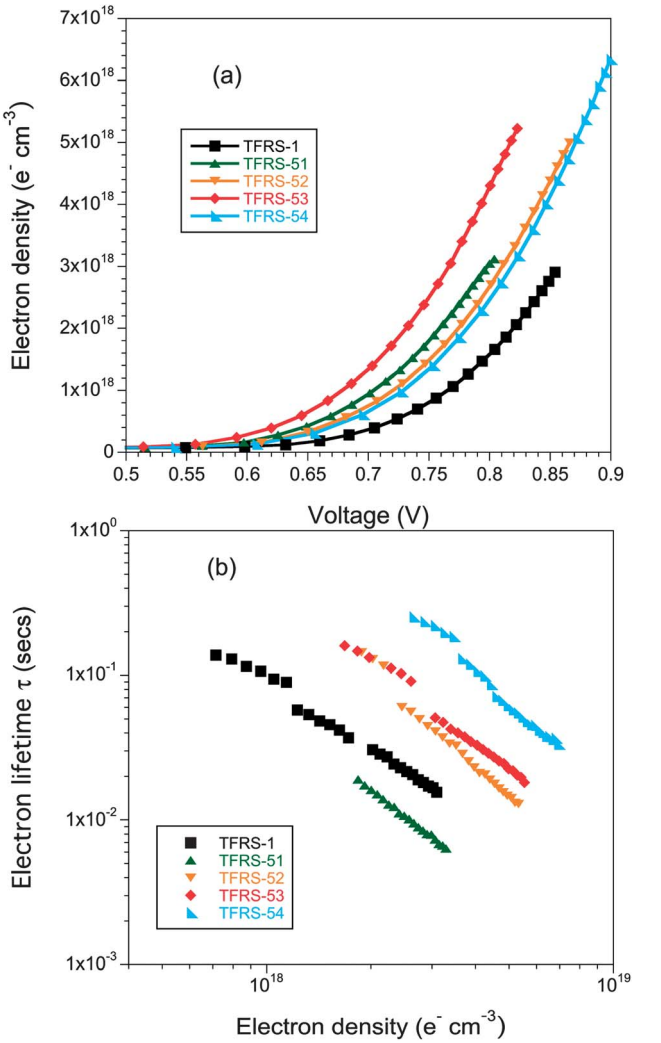

Fig. 5 (a) TiO_2 electron density *versus* voltage deduced from CE measurements and (b) electron lifetime τ *versus* TiO_2 electron density deduced from TPV measurements for DSC devices containing TFRS sensitizers. The cell voltage is induced *via* illumination from a series of LEDs.

account for the larger V_{OC} for these devices compared to the TFRS-1 device despite the downward shift in the conduction band.

From the TPV data it is also clear that the addition of the *t*-butyl groups slows down recombination in this series of sensitizers with TFRS-52 and TFRS-54 displaying longer electron lifetimes than their respective analogues that don't contain such groups (TFRS-51 and TFRS-53 respectively). A final point is that for all devices apart from the TFRS-51 device, the increase in conjugation of these complexes does not result in shorter electron lifetimes. This again indicates that increasing conjugation, as has been achieved with sensitizers TFRS-51–TFRS-54, and avoiding the introduction of groups containing heteroatoms such as sulfur, do not alter device electron lifetime and is a desired method to improve the light-harvesting of DSC devices without diminishing high V_{OC}.

Transient absorption measurements investigating charge recombination dynamics in DSC devices were next investigated in the presence and absence of electrolyte and are shown in Fig. 6 for DSC devices containing the representative TFRS-52 dye and also the reference dye TFRS-1. Dynamics for the other dyes can be found in the ESI.† In the absence of electrolyte all dyes show very similar multi-exponential behavior as has been observed previously for studies involving other Ru(II) polypyridine complexes.[49] In the presence of electrolyte the dynamics become biphasic as the dye cations are reduced by iodide in the electrolyte, resulting in the appearance of a long-lived signal assigned to electrons in the TiO_2 and/or $I_2^{\bullet-}$.[50] These kinetics indicate that regeneration for these Ru(II) complexes is slow and is the same for all of the TFRS dyes measured. Such slow kinetics cannot be due to small reaction driving force as the ground state oxidation potential for these dyes (*ca.* 0.9 V *vs.* NHE) is around 0.5 V higher than the I^-/I_3^- redox couple

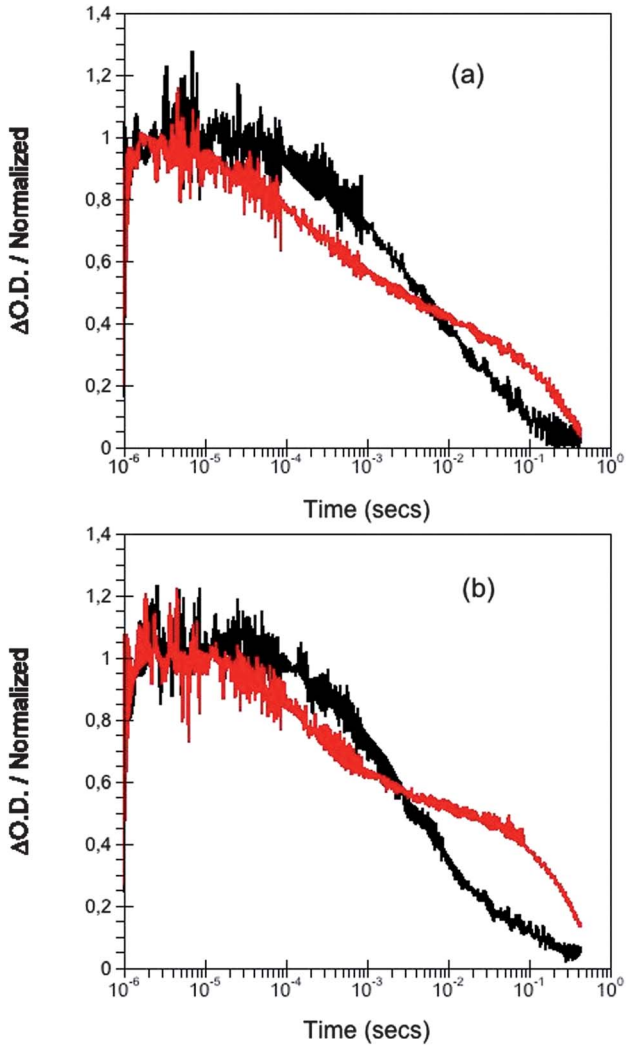

Fig. 6 Transient absorption decay kinetics of (a) TFRS-1 and (b) TFRS-52 devices in the presence (red) and absence (black) of redox electrolyte. Transient signals were recorded at 800 nm using laser excitation pulses of 500 nm kinetics.

(*ca.* 0.4 V *vs.* NHE).[38] Moreover, faster regeneration kinetics have been reported for Ru(II) complexes such as **C101** with similar oxidation potentials to the dyes used in this study.[51] Indeed, we have observed similar kinetics for a study involving a different class of bis-tridentate Ru(II) complexes.[52] Though in the case of the present study which involves tris–bidentate complexes, the common factor is the absence of thiocyanate groups and the complete chelation of the Ru(II) atom with bulky polypyridyl or relevant N-donor ligands. We therefore attribute such sluggish regeneration kinetics to the presence of these bulky ligands impeding interaction between iodide and the Ru(II) metal cation centered in these complexes.

Stability measurement

For testing long-term stability of DSCs at 60 °C, the electrolyte is modified to adopt excessive thermal and irradiative stresses. Thus, a low-volatility solvent, *i.e.* butyronitrile (BN), is used instead of the commonly used mixture of acetonitrile and valeronitrile. Besides, it is necessary to add guanidinium thiocyanate (GuNCS) into the electrolyte to stabilize the Pt counter electrode against attacks by iodine. Otherwise, gradual corrosion of Pt electrode results in an increase of series resistance at the electrolyte–Pt-FTO interface, giving a deteriorated fill factor, even though both of J_{SC} and V_{OC} exhibit minimal decline.[53] Therefore, we have selected two kinds of electrolytes; the electrolyte A consists of 1.0 M DMPII, 0.05 M iodine, 0.1 M GuNCS, and 0.5 M *N*-butyl-1*H*-benzimidazole (NBB) in BN, while the electrolyte B has the same composition except for an increased iodine concentration of 0.15 M. The performance evolution of both DSC devices is shown in Fig. 7 and Table 4.

As can be seen, both cells A and B display higher V_{OC} of 830 and 770 mV at $t = 0$ h, which are consistent with the cell using the less viscous electrolyte as shown in Table 4. Moreover, the device with electrolyte A showed a notable reduction of FF to 0.55 within the first 24 h and then recovered and stabilized at ~0.61 after 100 h. Such an observation is possibly attributed to the lower local concentration of tri-iodide in the electrolyte, causing an abrupt discontinuation of equilibrated tri-iodide concentration in the vicinity of the adsorbed dyes. It then slows down the tri-iodide diffused to the counter electrode, and hence giving higher series resistance and lower FF.[54] On the other hand, the increase in J_{SC} and without large loss of V_{OC} during light soaking is mainly due to a decrease in the conduction band energy and an increase in the injection rate and efficiency.[55]

Upon employment of electrolyte B with higher concentration of tri-iodide, the cell now shows a relatively lower and much more steady V_{OC} of 770 mV, higher J_{SC} of ~17 mA cm^{-2} and a higher FF of 0.68; all of these parameters showed much less deviation during a complete testing period of 1000 h. Despite this difference, both DSCs demonstrate satisfactory long-term

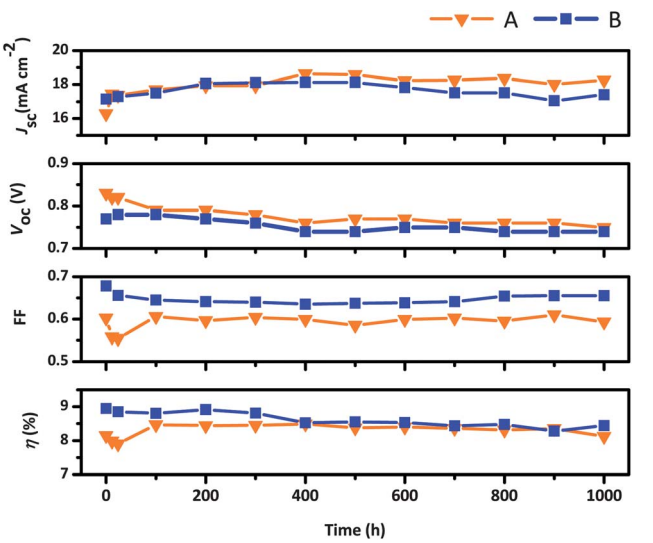

Fig. 7 Evolution of solar cell parameters of TFRS-52 measured under one sun light-soaking at 60 °C. Electrolyte A: 1.0 M DMPII, 0.05 M I_2, 0.1 M GuNCS, and 0.5 M NBB (*N*-butyl-1*H*-benzimidazole) in butyronitrile, while electrolyte B is modified by increasing I_2 concentration to 0.15 M.

Table 4 Selected performance data obtained during the light-soaking test

Electrolyte	Elapse (h)	J_{SC} [mA cm^{-2}]	V_{OC} [mV]	FF	η [%]	Overall decline
A	0	16.3	830	0.60	8.15	4.3%
	24	17.4	820	0.55	7.90	
	100	17.7	790	0.61	8.47	
	1000	18.3	750	0.59	8.12	
B	0	17.2	770	0.68	8.95	5.6%
	24	17.3	780	0.66	8.85	
	100	17.5	780	0.65	8.80	
	1000	17.4	740	0.65	8.44	

stabilities, which confirm the robust nature of TFRS-52 sensitizer under the current testing conditions.

Conclusion

Isoquinolinyl or quinolinyl functionalized ancillary chelates were incorporated into Ru(II)-based sensitizers for use in the fabrication of high efficiency DSCs. The increase in π-conjugation in the heterocyclic ancillaries of the sensitizers significantly improves the light-harvesting capabilities as well as the enhancement of J_{SC}. Thus, they represent a class of heterocycles with no chalcogen elements. These heterocyclic groups are known to exert less effective binding to iodine/tri-iodide in electrolyte solution, such that the recombination between photoinjected electrons in TiO_2 and acceptors in the electrolyte is minimized and, therefore, higher V_{OC} for the as-fabricated DSCs are expected. Moreover, the addition of *t*-butyl substituents to these structures results in longer device electron lifetimes indicating greater retardation of recombination losses of TiO_2 electrons to the electrolyte. Upon the *in situ* deprotonation of the carboxy anchors using the [TBA][DOC] treatment during absorption, devices with the highest V_{OC} of 860 mV have been achieved. Thus, the combination of these newly designed sensitizers and rational cell optimization using deprotonated co-adsorbants demonstrates a successful and facile method of increasing light absorption and J_{SC} whilst avoiding the often observed trade-off of lower V_{OC} due to increased recombination. This result echoes the general assumption that the V_{OC} could be the key parameter affecting the DSC performance.[56] The long-term stability test under light-soaking at 60 °C showed excellent stability by retaining ≥95% of its initial efficiency after 1000 h, which is satisfactory for future commercial applications.

Experimental

General procedures

All reactions were performed under argon atmosphere and solvents were distilled from appropriate drying agents prior to use. Commercially available reagents were used without further purification unless otherwise stated. All reactions were monitored using pre-coated TLC plates (0.20 mm with fluorescent indicator UV254). Mass spectra were obtained on a JEOL SX-102A instrument operating in electron impact (EI) or fast atom bombardment (FAB) mode. ^{1}H spectra were recorded on a Varian Mercury-400 instrument. Elemental analysis was carried out with a Heraeus CHN-O Rapid Elementary Analyzer.

Synthesis of 5-(6-*t*-butyl-1-isoquinolinyl)-3-trifluoromethyl pyrazole

To a stirred solution of $FeSO_4 \cdot 7H_2O$ (63 mg, 0.230 mmol) in CH_3CN was added paraacetaldehyde (9.0 mL, 67.6 mmol), 70% *t*-BuO_2H in water (4.6 mL, 33.8 mmol), 6-*tert*-butylisoquinoline (2.50 g, 13.5 mmol) and CF_3CO_2H (1.1 mL, 13.5 mmol). The mixture was refluxed for 12 h. After removing the solvent, the residue was taken up in saturated $Na_2CO_{3(aq)}$ (50 mL), extracted with ethyl acetate (3 × 50 mL), and concentrated to dryness. The product was purified by silica gel column chromatography (ethyl acetate/hexane = 1 : 8) to give a brown solid (1.58 g, 52%).

To a stirred solution of NaH (285 mg, 11.9 mmol) and THF (50 mL) at 0 °C was added a solution of 2-acetyl-6-*t*-butylisoquinoline (1.50 g, 6.61 mmol) in THF and ethyl trifluoroacetate (1.3 mL, 11.0 mmol) in sequence. The mixture was as refluxed for 12 h and then was neutralized with 2 M HCl until pH 4–5. After removing the solvent, the residue was extracted with CH_2Cl_2 (2 × 50 mL), washed with water, and concentrated to dryness to give a brown oil. Hydrazine monohydrate (3.2 mL, 66.1 mmol) in EtOH was added to the oily material in EtOH (50 mL). The solution was refluxed for 14 h. After removing the solvent, the residue was extracted with CH_2Cl_2 (2 × 50 mL), washed with water, and concentrated to dryness. The crude product was purified by silica gel column chromatography (ethyl acetate/hexane = 1 : 2) and recrystallized from hexane to give white solid (1.36 g, 65%).

Spectral data of 1-acetyl-6-*t*-butyl isoquinoline: MS (EI): *m*/*z* 319 $(M)^+$. ^{1}H NMR (400 MHz, $CDCl_3$, 298 K): δ 8.86 (d, J = 8.8 Hz, 1H), 8.52 (d, J = 6.0 Hz, 1H), 7.80–7.69 (m, 3H), 2.85 (s, 3H), 1.40 (s, 9H).

Spectral data of 5-(6-*t*-butyl-1-isoquinolinyl)-3-trifluoromethyl pyrazole: MS (EI): *m*/*z* 319 $(M)^+$. ^{1}H NMR (400 MHz, $CDCl_3$, 298 K): δ 12.82 (br, 1H), 8.48 (d, J = 5.6 Hz, 1H), 8.43 (d, J = 9.6 Hz, 1H), 7.82–7.75 (m, 2H), 7.66 (d, J = 5.6 Hz, 1H), 7.19 (s, 1H), 1.42 (s, 9H). ^{19}F NMR (376 MHz, $CDCl_3$, 298 K): δ −62.09 (s, 3F).

Synthesis of 5-(6-*tert*-butyl-2-quinolinyl)-3-trifluoromethyl pyrazole

The procedures are identical to those employed for isoquinolinyl derivatives. The acetylation and synthesis of pyrazole were obtained in 22 and 46% yields, respectively.

Spectral data of 2-acetyl-6-*t*-butyl quinoline: ^{1}H NMR (400 MHz, $CDCl_3$, 298 K): δ 8.19 (d, J = 8.4 Hz, 1H), 8.10 (d, J = 9.2 Hz, 1H), 8.08 (d, J = 8.4 Hz, 1H), 7.85 (dd, J = 9.2, 2.4 Hz, 1H), 7.75 (d, J = 2.4 Hz, 1H), 2.84 (s, 3H), 1.42 (s, 9H).

Spectral data of 5-(6-*t*-butyl-2-quinolinyl)-3-trifluoromethyl pyrazole: MS (EI): *m*/*z* 319 $(M)^+$. ^{1}H NMR (400 MHz, $CDCl_3$, 298 K): δ 11.63 (br, 1H), 8.20 (d, J = 8.4 Hz, 1H), 8.00 (d, J = 8.8 Hz, 1H), 7.84 (dd, J = 8.8, 2 Hz, 1H), 7.73 (d, J = 2.0 Hz, 1H), 7.68 (d, J = 8.4 Hz, 1H), 7.04 (s, 1H), 1.42 (s, 9H). ^{19}F NMR (376 MHz, $CDCl_3$, 298 K): δ −62.34 (s, 3F).

Synthesis of TFRS-51

5-(1-Isoquinolinyl)-3-trifluoromethyl pyrazole (87 mg, 0.330 mmol), [Ru(4,4′-bis(ethoxycarbonyl)-2,2′-bipyridine)(*p*-cymene)-Cl]Cl (100 mg, 0.165 mmol) and potassium acetate (81 mg, 0.824 mmol) were dissolved in xylenes (20 mL). The mixture was refluxed for 5 h. After removing the solvent, the residue was extracted with CH_2Cl_2 (3 × 25 mL), washed with water and concentrated to dryness. The mixture of products was purified by silica gel column chromatography (ethyl acetate/CH_2Cl_2 = 1 : 20) to give a black solid (55 mg, 34%).

Next, the solid product (37 mg, 0.0425 mmol) was dissolved in a mixture of acetone (20 mL) and 1 M NaOH solution (0.2 mL). The solution was heated to 60 °C under nitrogen for 3 h. After completing the hydrolysis, the solvent was removed under vacuum and the residue was dissolved in H_2O solution (10 mL). The solution was titrated with 2 M HCl to pH 3 to afford a dark brown precipitate. The dark brown precipitate was washed with deionized water, acetone and diethyl ether in sequence, giving dark brown solid (30 mg, 87%).

Spectral data of TFRS-51: MS (FAB, ^{102}Ru): *m*/*z* 870 $(M)^+$. ^{1}H NMR (400 MHz, d_6-DMSO, 298 K): δ 9.00 (s, 2H), 8.91 (d, J = 5.6 Hz, 2H), 8.09 (d, J = 5.6 Hz, 2H), 7.94–7.86 (m, 4H), 7.82–7.72 (m, 6H), 7.62 (d, J = 6.4 Hz, 2H), 7.06 (d, J = 6.4 Hz, 2H). ^{19}F NMR (376 MHz, d_6-DMSO, 298 K): δ −58.01 (s, 6F). Anal. Calcd. for $C_{38}H_{22}F_6N_8O_4Ru \cdot H_2O$: C, 51.41; N, 12.62; H, 2.73. Found: C, 51.24; N, 12.33; H, 2.94%.

Synthesis of TFRS-52–TFRS-54

The same procedure was used as in the synthesis of TFRS-51, starting from the relevant pyrazole chelate. The ester derivatives of TFRS-52–TFRS-54 were first obtained in 32–38% yield. Further treatment with NaOH in mixture of acetone and water afforded the hydrolyzed TFRS-52–TFRS-54 in 89–92% yield.

Spectral data of TFRS-52: MS (FAB, ^{102}Ru): *m*/*z* 982 $(M)^+$. ^{1}H NMR (400 MHz, d_6-DMSO, 298 K): δ 8.99 (s, 2H), 8.81 (d, J = 9.2 Hz, 2H), 8.12 (d, J = 5.6 Hz, 2H), 7.86 (dd, J = 9.2, 2 Hz, 2H), 7.81 (d, J = 2.0 Hz, 2H), 7.80 (s, 2H), 7.73 (dd, J = 5.6, 2.0 Hz, 2H), 7.56 (d, J = 6.4 Hz, 2H), 7.02 (d, J = 6.4 Hz, 2H), 1.35 (s, 9H). ^{19}F NMR (376 MHz, d_6-DMSO, 298 K): δ −58.00 (s, 6F). Anal. Calcd. for $C_{46}H_{38}F_6N_8O_4Ru \cdot H_2O$: C, 55.25; N, 11.21; H, 4.03. Found: C, 55.21; N, 11.44; H, 4.28%.

Spectral data of TFRS-53: MS (FAB, ^{102}Ru): *m*/*z* 871 $(M + 1)^+$. ^{1}H NMR (400 MHz, d_6-DMSO, 298 K): δ 9.06 (s, 2H), 8.28 (d, J = 6.0 Hz, 2H), 8.20 (d, J = 8.4 Hz, 2H), 7.90 (d, J = 8.4 Hz, 2H), 7.79 (d, J = 7.6 Hz, 2H), 7.68 (d, J = 6.0 Hz, 2H), 7.41 (s, 2H), 7.38 (t, J = 7.6 Hz, 2H), 7.05 (t, J = 7.6 Hz, 2H), 6.78 (d, J = 8.8 Hz, 2H). ^{19}F NMR (376 MHz, d_6-DMSO, 298 K): δ −58.07 (s, 6F). Anal. Calcd. for $C_{38}H_{22}F_6N_8O_4Ru \cdot H_2O$: C, 51.41; N, 12.62; H, 2.73. Found: C, 51.17; N, 12.16; H, 3.03%.

Spectral data of TFRS-54: MS (FAB, ^{102}Ru): *m*/*z* 983 $(M + 1)^+$. ^{1}H NMR (400 MHz, d_6-DMSO, 298 K): δ 9.00 (s, 2H), 8.27 (d, J = 8.8 Hz, 2H), 8.11 (d, J = 6.0 Hz, 2H), 8.00 (d, J = 8.4 Hz, 2H), 7.78 (d, J = 2.0 Hz, 2H), 7.68 (dd, J = 6.0, 1.6 Hz, 2H), 7.46 (s, 2H), 7.08 (dd, J = 9.2, 2.4 Hz, 2H), 6.69 (d, J = 9.6 Hz, 2H), 1.24 (s, 9H). ^{19}F NMR (376 MHz, d_6-DMSO, 298 K): δ −58.14 (s, 6F). Anal. Calcd. for $C_{46}H_{38}F_6N_8O_4Ru \cdot 2H_2O$: C, 54.28; N, 11.01; H, 4.16. Found: C, 54.13; N, 10.87; H, 4.16%.

Theoretical calculations

All calculations were performed using the Gaussian 09 program package.[57] Their ground state structures were first optimized with density functional theory (DFT) at B3LYP/LANL2DZ (Ru) and 6-31G* (H, C, N, O, S, F) level. The optimized structures were then used to calculate 60 lowest singlet energy optical excitations using the time-dependent density functional theory (TD-DFT) method. A polarizable continuum model (PCM) in Gaussian 09 was applied using DMF as the solvent.

Device fabrication

Fluorine-doped tin oxide (FTO) coated glasses (3.2 mm thickness, sheet resistance of 9 Ω cm^{-2}, Pilkington) were washed with detergent, water, acetone and ethanol in sequence and then dried under nitrogen. After treatment in a UV–O_3 system for 15 min (PSD series UV-ozone cleaning, Novascan Technologies, Inc.), the FTO glass plates were immersed into a 40 mM aqueous $TiCl_4$ solution at 70 °C for 30 min and rinsed with water and ethanol. The photoanodes composed of nanocrystalline TiO_2 were prepared using literature procedures.[58] The 12 μm of 20 nm TiO_2 layer and a 6 μm light-scattering layer containing 400 nm TiO_2 particles (PST-400, JGC Catalysts and Chemicals, Japan) were screen-printed (active area, 0.4 × 0.4 cm^2). The TiO_2 electrodes were heated under an air flow at 325 °C for 30 min, followed by heating at 375 °C for 5 min, 450 °C for 15 min, and 500 °C for 30 min. The TiO_2 electrodes were treated with a 40 mM aqueous solution of $TiCl_4$ at 70 °C for 30 min and then washed with water and ethanol. The electrodes were sintered again at 500 °C for 30 min and left to cool to 80 °C before dipping them into the dye solution (0.3 mM) for 18 h at 25 °C. The dye solution was prepared in absolute ethanol with 20% (v/v) of DMSO with/without addition of 2 equiv. of tetrabutylammonium deoxycholate [TBA][DOC] as coadsorbent. The Pt-coated counter electrodes were prepared by dropping 10 μL of H_2PtCl_6 solution (5 mM) in isopropyl alcohol on pre-drilled FTO glass plates (15 × 15 mm^2) and heated up to 400 °C for 15 min The dye-sensitized TiO_2 electrodes were assembled with Pt counter electrodes by inserting a hot-melt Surlyn film (Meltonix 1170-25, 25 μm, Solaronix) as spacer between the electrodes, and then heated at 130 °C. The electrolyte solution, which consists of 0.6 M 1,2-dimethyl-3-propylimidazolium iodide (DMPII), 0.05 M iodine, and 0.5 M *t*-butylpyridine (TBP) in a 15 : 85 (v/v) mixture of valeronitirile and acetonitrile, is injected into the cell through a pre-drilled hole at the counter electrode. Finally, the hole was sealed using a hot-melt Surlyn film and a cover glass. In order to reduce the light from entering the cell,[59] all devices were covered with a light-shading mask with size of 0.6 × 0.6 cm^2.

Photovoltaic characterization

Photovoltaic measurements were recorded with a Newport Oriel Class A Solar Simulator (Model 91159) equipped with a class A 150 W xenon light source powered by a Newport power supply

(Model 69907). The light output (area: 2 × 2 inch^2) was calibrated to AM 1.5 using a Newport Oriel correction filter to reduce the spectra mismatch in the region of 350–750 nm to less than 4%. The power output of the lamp was turned to 1 Sun (100 mW cm^{-2}) using a certified Si reference cell (SRC–1000–TC–QZ, VLSI standard S/N: 10510-0031). The current voltage characteristic was obtained by applying an external potential bias to the cell and measuring the generated photocurrent with a Keithley digital source meter (Model 2400). The spectra of incident photon-to-current conversion efficiency (IPCE) were calculated using the equation $1240J_{SC}(\lambda)/(\lambda P_{in}(\lambda))$ and were plotted as a function of incident wavelength with an increment of 10 nm. It should be noted that 20 sets of J_{SC} (interval 50 ms) were collected after each illumination of 3 seconds and were averaged for calculation of IPCE.[60] A 300 W Xe lamp (Model 6258, Newport Oriel) combined with an Oriel cornerstone 260 1/4 m monochromator (Model 74100) provided an unchopped monochromatic beam onto a photovoltaic cell. The beam intensity was calibrated with a power meter (Model 1936-C, Newport) equipped with a Newport 818-UV photodetector.

Loading of sensitizer

The dye loading on 12 + 6 μm TiO_2 films was calculated by dipping the TiO_2 film into 0.1 M tetra-*n*-butyl ammonium hydroxide solution in MeOH and H_2O (v/v 1 : 1) for dye desorbing and then measured their absorbance using the UV/Vis spectral analysis.

Charge extraction and transient photovoltage measurements

Transient photovoltage (TPV) and charge extraction (CE) measurements were carried out on optimized 0.16 cm^2 DSC devices using a system similar to that employed by O'Regan *et al.*[61]

Transient absorption spectroscopy measurements

Transient absorption spectroscopy (TAS) measurements were carried out on 1 cm^2 DSC devices on a system similar to that used by Durrant and co-workers.[49]

Electrical impedance measurements

Electrical impedance experiments were carried out with a PARSTAT 2273 (AMETEK Princeton Applied Research, USA) electrochemical workstation, with a frequency range of $0.05-10^6$ Hz and a potential modulation of 10 mV at room temperature.

Stability test

The devices employed in this study are composed of a 12 μm transparent TiO_2 thin film and a 6 μm thick layer of 400 nm TiO_2 particles. A 370 nm cut-off long pass filter film was applied to the front surface during illumination and Al foil was covered on the surrounding glass of device. The cell was placed under a Suntest CPS plus lamp (ATLAS GmbH, 100 mW cm^{-2}) during visible-light soaking at 60 °C. The electrolyte A consists of 1.0 M DMPII, 0.05 M iodine, 0.1 M GNCS, and 0.5 M NBB (*N*-butyl-1*H*-benzimidazole) in butyronitrile (BN)[53] and electrolyte B has the identical composition except for an increased iodine concentration of 0.15 M.

Acknowledgements

This work was supported by the National Science Council of Taiwan under grant NSC 100-2119-M-002-008, and the National Center for High-Performance Computing for computer time and facilities. EP would like to thank the financial support from ICIQ, ICREA, the Spanish MICINN projects CTQ2010-18859 and CONSOLIDER CDS-0007 HOPE-2007, the EU for the ERCstg Polydot, and the Catalan government for the 2009-SGR-207 project. JNC thanks the MICINN for the Juan de la Cierva Fellowship. K.-L.W. is a recipient of the exchange scholarship sponsored by National Science Council of Taiwan (NSC-101-2917-I-007-017).

References

1 L. M. Goncalves, V. de Zea Bermudez, H. A. Ribeiro and A. M. Mendes, *Energy Environ. Sci.*, 2008, **1**, 655.
2 G. C. Vougioukalakis, A. I. Philippopoulos, T. Stergiopoulos and P. Falaras, *Coord. Chem. Rev.*, 2011, **255**, 2602.
3 Y.-S. Yen, H.-H. Chou, Y.-C. Chen, C.-Y. Hsu and J. T. Lin, *J. Mater. Chem.*, 2012, **22**, 8734.
4 Y. Ooyama and Y. Harima, *Eur. J. Org. Chem.*, 2009, 2903.
5 Z. Ning, Y. Fu and H. Tian, *Energy Environ. Sci.*, 2010, **3**, 1170.
6 A. Hagfeldt and M. Grätzel, *Acc. Chem. Res.*, 2000, **33**, 269.
7 M. K. Nazeeruddin, P. Pechy, T. Renouard, S. M. Zakeeruddin, R. Humphry-Baker, P. Comte, P. Liska, L. Cevey, E. Costa, V. Shklover, L. Spiccia, G. B. Deacon, C. A. Bignozzi and M. Grätzel, *J. Am. Chem. Soc.*, 2001, **123**, 1613.
8 M. Grätzel, *Inorg. Chem.*, 2005, **44**, 6841.
9 M. K. Nazeeruddin, S. M. Zakeeruddin, R. Humphry-Baker, M. Jirousek, P. Liska, N. Vlachopoulos, V. Shklover, C.-H. Fischer and M. Grätzel, *Inorg. Chem.*, 1999, **38**, 6298.
10 S. Fantacci and F. De Angelis, *Coord. Chem. Rev.*, 2011, **255**, 2704.
11 A. Reynal and E. Palomares, *Eur. J. Inorg. Chem.*, 2011, 4509.
12 P. Xie and F. Guo, *Curr. Org. Chem.*, 2011, **15**, 3849.
13 M. K. Nazeeruddin, E. Baranoff and M. Grätzel, *Sol. Energy*, 2011, **85**, 1172.
14 Y. Cao, Y. Bai, Q. Yu, Y. Cheng, S. Liu, D. Shi, F. Gao and P. Wang, *J. Phys. Chem. C*, 2009, **113**, 6290.
15 C.-Y. Chen, M. Wang, J.-Y. Li, N. Pootrakulchote, L. Alibabaei, C.-H. Ngoc-Le, J.-D. Decoppet, J.-H. Tsai, C. Grätzel, C.-G. Wu, S. M. Zakeeruddin and M. Grätzel, *ACS Nano*, 2009, **3**, 3103.
16 M. K. Nazeeruddin, F. De Angelis, S. Fantacci, A. Selloni, G. Viscardi, P. Liska, S. Ito, B. Takeru and M. Grätzel, *J. Am. Chem. Soc.*, 2005, **127**, 16835.
17 H.-J. Koo, Y. J. Kim, Y. H. Lee, W. I. Lee, K. Kim and N.-G. Park, *Adv. Mater.*, 2008, **20**, 195.
18 B. C. O'Regan, K. Walley, M. Juozapavicius, A. Anderson, F. Matar, T. Ghaddar, S. M. Zakeeruddin, C. Klein and J. R. Durrant, *J. Am. Chem. Soc.*, 2009, **131**, 3541.

19 J. N. Clifford, E. Martinez-Ferrero and E. Palomares, *J. Mater. Chem.*, 2012, **22**, 12415.
20 Y. Bai, J. Zhang, D. Zhou, Y. Wang, M. Zhang and P. Wang, *J. Am. Chem. Soc.*, 2011, **133**, 11442.
21 T. Marinado, K. Nonomura, J. Nissfolk, M. K. Karlsson, D. P. Hagberg, L. Sun, S. Mori and A. Hagfeldt, *Langmuir*, 2010, **26**, 2592.
22 H. Kusama and K. Sayama, *J. Phys. Chem. C*, 2012, **116**, 1493.
23 X. Zong, M. Liang, T. Chen, J. Jia, L. Wang, Z. Sun and S. Xue, *Chem. Commun.*, 2012, **48**, 6645.
24 C. Giordano, F. Minisci, E. Vismara and S. Levi, *J. Org. Chem.*, 1986, **51**, 536.
25 M.-W. Chung, T.-Y. Lin, C.-C. Hsieh, K.-C. Tang, H. Fu, P.-T. Chou, S.-H. Yang and Y. Chi, *J. Phys. Chem. A*, 2010, **114**, 7886.
26 M. Kato, K. Sasano, C. Kosuge, M. Yamazaki, S. Yano and M. Kimura, *Inorg. Chem.*, 1996, **35**, 116.
27 M. Jaeger, L. Eriksson, J. Bergquist and O. Johansson, *J. Org. Chem.*, 2007, **72**, 10227.
28 R. F. Semeniuc, T. J. Reamer and M. D. Smith, *New J. Chem.*, 2010, **34**, 439.
29 A. L. Smith, F. F. De Morin, N. A. Paras, Q. Huang, J. K. Petkus, E. M. Doherty, T. Nixey, J. L. Kim, D. A. Whittington, L. F. Epstein, M. R. Lee, M. J. Rose, C. Babij, M. Fernando, K. Hess, Q. Le, P. Beltran and J. Carnahan, *J. Med. Chem.*, 2009, **52**, 6189.
30 R. Tan, P. Jia, Y. Rao, W. Jia, A. Hadzovic, Q. Yu, X. Li and D. Song, *Organometallics*, 2008, **27**, 6614.
31 K.-L. Wu, H.-C. Hsu, K. Chen, Y. Chi, M.-W. Chung, W.-H. Liu and P.-T. Chou, *Chem. Commun.*, 2010, **46**, 5124.
32 P.-C. Wu, J.-K. Yu, Y.-H. Song, Y. Chi, P.-T. Chou, S.-M. Peng and G.-H. Lee, *Organometallics*, 2003, **22**, 4938.
33 K.-L. Wu, S.-T. Ho, C.-C. Chou, Y.-C. Chang, H.-A. Pan, Y. Chi and P.-T. Chou, *Angew. Chem., Int. Ed.*, 2012, **51**, 5642.
34 C.-W. Hsu, S.-T. Ho, K.-L. Wu, Y. Chi, S.-H. Liu and P.-T. Chou, *Energy Environ. Sci.*, 2012, **5**, 7549.
35 C.-C. Chou, K.-L. Wu, Y. Chi, W.-P. Hu, S. J. Yu, G.-H. Lee, C.-L. Lin and P.-T. Chou, *Angew. Chem., Int. Ed.*, 2011, **50**, 2054.
36 J. L. Segura, H. Herrera and P. Baeuerle, *J. Mater. Chem.*, 2012, **22**, 8717.
37 S.-Y. Chang, J. Kavitha, J.-Y. Hung, Y. Chi, Y.-M. Cheng, E. Y. Li, P.-T. Chou, G.-H. Lee and A. J. Carty, *Inorg. Chem.*, 2007, **46**, 7064.
38 A. Hagfeldt, G. Boschloo, L. Sun, L. Kloo and H. Pettersson, *Chem.–Eur. J.*, 2010, **110**, 6595.
39 Y. Cui, Y. Wu, X. Lu, X. Zhang, G. Zhou, F. B. Miapeh, W. Zhu and Z.-S. Wang, *Chem. Mater.*, 2011, **23**, 4394.
40 K. Pei, Y. Wu, W. Wu, Q. Zhang, B. Chen, H. Tian and W. Zhu, *Chem.–Eur. J.*, 2012, **18**, 8190.
41 C. Li, J.-H. Yum, S.-J. Moon, A. Herrmann, F. Eickemeyer, N. G. Pschirer, P. Erk, J. Schoeneboom, K. Muellen, M. Grätzel and M. K. Nazeeruddin, *ChemSusChem*, 2008, **1**, 615.
42 J.-H. Yum, D. P. Hagberg, S.-J. Moon, K. M. Karlsson, T. Marinado, L. Sun, A. Hagfeldt, M. K. Nazeeruddin and M. Grätzel, *Angew. Chem., Int. Ed.*, 2009, **48**, 1576.
43 D.-Y. Chen, Y.-Y. Hsu, H.-C. Hsu, B.-S. Chen, Y.-T. Lee, H. Fu, M.-W. Chung, S.-H. Liu, H.-C. Chen, Y. Chi and P.-T. Chou, *Chem. Commun.*, 2010, **46**, 5256.
44 Y. Wu, X. Zhang, W. Li, Z.-S. Wang, H. Tian and W. Zhu, *Adv. Energy Mater.*, 2012, **2**, 149.
45 N. R. Neale, N. Kopidakis, J. van de Lagemaat, M. Grätzel and A. J. Frank, *J. Phys. Chem. B*, 2005, **109**, 23183.
46 M. K. Nazeeruddin, R. Humphry-Baker, P. Liska and M. Grätzel, *J. Phys. Chem. B*, 2003, **107**, 8981.
47 F. Fabregat-Santiago, J. Bisquert, G. Garcia-Belmonte, G. Boschloo and A. Hagfeldt, *Sol. Energy Mater. Sol. Cells*, 2005, **87**, 117.
48 M. S. Goes, E. Joanni, E. C. Muniz, R. Savu, T. R. Habeck, P. R. Bueno and F. Fabregat-Santiago, *J. Phys. Chem. C*, 2012, **116**, 12415.
49 J. N. Clifford, E. Palomares, M. K. Nazeeruddin, M. Grätzel, J. Nelson, X. Li, N. J. Long and J. R. Durrant, *J. Am. Chem. Soc.*, 2004, **126**, 5225.
50 I. Montanari, J. Nelson and J. R. Durrant, *J. Phys. Chem. B*, 2002, **106**, 12203.
51 M. Garcia-Iglesias, L. Pelleja, J.-H. Yum, D. Gonzalez-Rodriguez, M. K. Nazeeruddin, M. Graetzel, J. N. Clifford, E. Palomares, P. Vazquez and T. Torres, *Chem. Sci.*, 2012, **3**, 1177.
52 K.-L. Wu, C.-H. Li, Y. Chi, J. N. Clifford, L. Cabau, E. Palomares, Y.-M. Cheng, H.-A. Pan and P.-T. Chou, *J. Am. Chem. Soc.*, 2012, **134**, 7488.
53 F. Sauvage, S. Chhor, A. Marchioro, J.-E. Moser and M. Grätzel, *J. Am. Chem. Soc.*, 2011, **133**, 13103.
54 G. Boschloo and A. Hagfeldt, *Acc. Chem. Res.*, 2009, **42**, 1819.
55 A. Listorti, C. Creager, P. Sommeling, J. Kroon, E. Palomares, A. Fornelli, B. Breen, P. R. F. Barnes, J. R. Durrant, C. Law and B. O'Regan, *Energy Environ. Sci.*, 2011, **4**, 3494.
56 T. Stergiopoulos and P. Falaras, *Adv. Energy Mater.*, 2012, **2**, 616.
57 M. J. Frisch, G. W. Trucks, H. B. Schlegel, G. E. Scuseria, M. A. Robb, J. R. Cheeseman, G. Scalmani, V. Barone, B. Mennucci, G. A. Petersson, H. Nakatsuji, M. Caricato, X. Li, H. P. Hratchian, A. F. Izmaylov, J. Bloino, G. Zheng, J. L. Sonnenberg, M. Hada, M. Ehara, K. Toyota, R. Fukuda, J. Hasegawa, M. Ishida, T. Nakajima, Y. Honda, O. Kitao, H. Nakai, T. Vreven, J. A. Montgomery, J. E. Peralta, F. Ogliaro, M. Bearpark, J. J. Heyd, E. Brothers, K. N. Kudin, V. N. Staroverov, R. Kobayashi, J. Normand, K. Raghavachari, A. Rendell, J. C. Burant, S. S. Iyengar, J. Tomasi, M. Cossi, N. Rega, J. M. Millam, M. Klene, J. E. Knox, J. B. Cross, V. Bakken, C. Adamo, J. Jaramillo, R. Gomperts, R. E. Stratmann, O. Yazyev, A. J. Austin, R. Cammi, C. Pomelli, J. W. Ochterski, R. L. Martin, K. Morokuma, V. G. Zakrzewski, G. A. Voth, P. Salvador, J. J. Dannenberg, S. Dapprich, A. D. Daniels, J. B. Farkas Foresman, J. V. Ortiz, J. Cioslowski and D. J. Fox, Gaussian 09, Wallingford CT, 2009.
58 S. Ito, T. N. Murakami, P. Comte, P. Liska, C. Grätzel, M. K. Nazeeruddin and M. Grätzel, *Thin Solid Films*, 2008, **516**, 4613.

59 S. Ito, K. Nazeeruddin, P. Liska, P. Comte, R. Charvet, P. Pechy, M. Jirousek, A. Kay, S. M. Zakeeruddin and M. Grätzel, *Progr. Photovolt.: Res. Appl.*, 2006, **14**, 589.
60 X.-Z. Guo, Y.-H. Luo, Y.-D. Zhang, X.-C. Huang, D.-M. Li and Q.-B. Meng, *Rev. Sci. Instrum.*, 2010, **81**, 103106.
61 B. C. O'Regan, K. Bakker, J. Kroeze, H. Smit, P. Sommeling and J. R. Durrant, *J. Phys. Chem. B*, 2006, **110**, 17155.

